OPEN

Optical Imaging of Drug-Induced Metabolism Changes in Murine and Human Pancreatic Cancer Organoids Reveals Heterogeneous Drug Response

Alex J. Walsh, PhD, Jason A. Castellanos, MD,† Nagaraj S. Nagathihalli, PhD,‡§|| Nipun B. Merchant, MD,‡§|| and Melissa C. Skala, PhD**

Objectives: Three-dimensional organoids derived from primary pancreatic ductal adenocarcinomas are an attractive platform for testing potential anticancer drugs on patient-specific tissue. Optical metabolic imaging (OMI) is a novel tool used to assess drug-induced changes in cellular metabolism, and its quantitative end point, the OMI index, is evaluated as a biomarker of drug response in pancreatic cancer organoids.

Methods: Optical metabolic imaging is used to assess both malignant cell and fibroblast drug response within primary murine and human pancreatic cancer organoids.

Results: Anticancer drugs induce significant reductions in the OMI index of murine and human pancreatic cancer organoids. Subpopulation analysis of OMI data revealed heterogeneous drug response and elucidated responding and nonresponding cell populations for a 7-day time course. Optical metabolic imaging index significantly correlates with immunofluorescence detection of cell proliferation and cell death.

Conclusions: Optical metabolic imaging of primary pancreatic ductal adenocarcinoma organoids is highly sensitive to drug-induced metabolic changes, provides a nondestructive method for monitoring dynamic drug response, and presents a novel platform for patient-specific drug testing and drug development.

Key Words: pancreatic ductal adenocarcinoma, organoids, cellular metabolism, optical microscopy

(*Pancreas* 2016;45: 863–869)

Primary tissue–derived organoids are an attractive platform for studying disease progression, invasion, and drug response.[1–3] Primary ductal adenocarcinoma (PDAC) organoids have the same protein and genetic abnormalities as malignant disease[2] and better replicate tumor behaviors than 2-dimensional cultures of cells. In addition, hundreds to thousands of organoids can be generated from a single tissue biopsy, which allows for high-throughput screening of organoid behaviors in response to perturbations. Therefore, organoids provide a relevant system for testing drug response for individualized treatment planning and novel drug discovery.

From the *Department of Biomedical Engineering, Vanderbilt University; and †Department of Surgery, Vanderbilt University School of Medicine, Nashville, TN; ‡Sylvester Comprehensive Cancer Center, University of Miami; and §Division of Surgical Oncology and ||Department of Surgery, University of Miami Miller School of Medicine, Miami, FL.

Received for publication May 7, 2015; accepted August 7, 2015.

Reprints: Melissa C. Skala, PhD, Department of Biomedical Engineering, Vanderbilt University, Station B Box 1631, Nashville, TN 37235 (e-mail: m.skala@vanderbilt.edu).

This study was supported by NIH/NCI R01-CA185747 and NIH/NCI R01-CA161976 (N.B.M.).

The authors declare no conflict of interest.

Optical imaging is well suited for imaging organoids due to its high spatial resolution, functional contrast, and depth of imaging. Optical metabolic imaging (OMI) is a novel, nondestructive method of imaging and quantifying drug-induced changes in cellular metabolism.[3–5] Optical metabolic imaging probes the autofluorescence intensity and lifetime of NAD(P)H and FAD for robust detection of cellular metabolic states. The OMI end point, the optical redox ratio, is the fluorescence intensity of NAD(P)H divided by the intensity of FAD and measures the redox state of the cell.[6,7] The fluorescence lifetime is the time a fluorophore remains in the excited state and is altered by protein conformation changes, proximity to quenchers, and preferred protein binding. A comprehensive analysis of cellular metabolism can be obtained by probing NAD(P)H and FAD fluorescence intensity and lifetime.[4] Furthermore, OMI is well suited for evaluating heterogeneous drug response due to its single-cell resolution and high sensitivity to changes in cellular metabolism.

The OMI index, a composite end point of NAD(P)H and FAD fluorescence properties, was developed to directly correlate metabolism changes with drug response. The OMI index is a linear combination of mean-centered optical redox ratio, NAD(P)H fluorescence lifetime, and FAD fluorescence lifetime data, computed for each cell within a data set. The OMI index allows comparison of metabolic states across experimental groups, with significant decreases in OMI index indicating drug response.[3] In this study, the OMI index is evaluated as a robust and highly sensitive biomarker for drug response in PDAC organoids, derived from both primary murine and human tumors.

MATERIALS AND METHODS

Mouse Organoid Generation and Culture

This study was approved by the Vanderbilt University Animal Care and Use Committee and meets the National Institutes of Health guidelines for animal welfare. Sections of PDAC were resected from 3 PKT ($Ptf1a^{cre/+}$;LSL-$Kras^{G12D/+}$;$Tgfbr2^{flox/flox}$) mice.[8] Tumor sections were washed 3 times with phosphate buffered saline (PBS) and placed in 0.5-mL Roswell Park Memorial Institute media supplemented with 10% fetal bovine serum, 1% penicillin-streptomycin, and 10-ng/mL epidermal growth factor receptor, hereafter referred to as PDAC organoid media. Organoids were generated by mechanical dissociation of the tumor sections with surgical scissors and a scalpel. The resulting solution was filtered to exclude tissue sections larger than 500 μm in diameter and mixed with Matrigel 1:2. Gels were allowed to solidify at room temperature for 30 minutes and in an incubator for 1 hour. Then, media were added to cover each gel. Organoids grew for 3 days and then were treated with the following drugs and drug combinations: control (dimethyl sulfoxide), gemcitabine (G; 25 μg/mL), AZD1480 (A1; 100 nM), AZD6244 (A6; 4 μM), XL147 (X; 25 nM), G + A1, G + A1 + A6, and G + A1 + A6 + X. Media were replaced every 3 days.

Human Organoid Generation and Culture

This study was approved by the Vanderbilt University Institutional Review Board. A primary tumor biopsy was obtained from a patient with poorly differentiated pancreatic ductal adenocarcinoma during a Whipple procedure (pancreaticoduodenectomy). The tumor section was placed in PDAC organoid media and transported on ice to the optical imaging laboratory, ~5-minute walk. Previous studies of organoid generation and OMI end points confirm tissue viability and metabolic end point congruity within this time frame.[3,9] The tissue sample was washed 3 times with PBS and placed in 0.5 mL of PDAC organoid media. Organoids were generated by mechanical dissociation with surgical scissors and a scalpel, in the same procedure as the mouse tissue. The tissue sections were filtered to remove tissue sections larger than 500 μm in diameter and mixed with Matrigel 1:2. Gels were allowed to solidify at room temperature for 30 minutes and in an incubator for 1 hour. Then, PDAC organoid media were added to cover each gel. Organoids grew for 3 days and then were treated with the following drugs and drug combinations: control (dimethyl sulfoxide), G (25 μg/mL), A1 (100 nM), and G + A1. Media were replaced every 3 days.

Optical Metabolic Imaging

Optical metabolic imaging probes the fluorescence intensity and lifetime of NAD(P)H and FAD. NAD(P)H and FAD are coenzymes used in multiple cellular metabolism processes including glycolysis and oxidative phosphorylation. The end points of OMI include the redox ratio, NAD(P)H fluorescence lifetime, FAD fluorescence lifetime, and a combination variable, the OMI index. The redox ratio is the intensity of NAD(P)H fluorescence relative to the intensity of FAD fluorescence and provides information on the relative amounts of electron donors and acceptors in the cell.[6,10] The redox ratio is sensitive to shifts in metabolic pathways.[4,10] The fluorescence lifetimes report changes in the microenvironment of NAD(P)H and FAD and are especially sensitive to the binding state of the fluorophore, as well as local temperature, pH, and proximity to quenchers such as molecular oxygen.[11] Both NAD(P)H and FAD fluorescence lifetimes can be either short or long, depending on the binding state of NAD(P)H and FAD (free or bound to an enzyme complex).[12,13] Previous studies have shown that OMI end points are sensitive to metabolism differences between cancer subtypes.[3,4,14] In addition, the OMI end points provide dynamic readouts of cellular metabolism and detect premalignant transformations within tissues,[5,15] classify subtypes of breast cancer cells,[4,14] and detect response to anticancer drugs.[3]

Fluorescence lifetime imaging was performed on a custom-built multiphoton microscope adapted for lifetime imaging, as previously described.[3,4,9] Laser excitation light was provided by a Titanium:Sapphire laser (Coherent, Inc, Santa Clara, Calif) tuned to 750 nm to excite NAD(P)H (average power, ~7.5–8 mW at the sample) and 890 nm to excite FAD (average power, ~8.1–8.5 mW at the sample). Excitation and emission light was coupled through a 40× oil immersion objective (1.3 NA) within an inverted microscope (Nikon TiE, Tokyo, Japan). Customized filter cubes isolated NAD(P)H emission between 400 and 480 nm and FAD emission between 500 and 600 nm. Fluorescence lifetime imaging was performed with time-correlated single-photon counting electronics (Becker and Hickl SPC-150; Berlin, Germany) and a GaAsP PMT (Hamamatsu H7422P-40; Hamamatsu City, Japan). A 4.6-μs-pixel dwell time was used to acquire 256 × 256 pixel images. Fluorescence lifetime images were acquired for 60 seconds, with the photon count rate maintained greater than 5×10^5, ensuring no photobleaching occurred and adequate photon observations for lifetime decay fitting. The instrument response function full width at half maximum was 260 ps as measured from the second harmonic generation of a urea crystal. Daily fluorescence lifetime measurements were validated by imaging of a YG fluorescent bead (Polysciences, Inc, Warrington, Pa). The measured lifetime of the bead, 2.1 ± 0.04 ns, agrees with published values.[3,4]

To ensure spectral isolation of NAD(P)H and FAD, we performed a cyanide experiment[4] in which cells were exposed to 4-nM NaCN. Cyanide disrupts cellular metabolism and should result in an increased NAD(P)H concentration/fluorescence signal and a decreased FAD concentration/fluorescence signal in the first minutes after exposure.[16] FAD images were examined for strong pixelated fluorescence signals with very short lifetimes, as would be apparent from lipofuscin granules, to ensure no fluorescence contributions from lipofuscin in the FAD images.

Organoid Imaging

Images of NAD(P)H and FAD fluorescence lifetimes were acquired on 1, 2, 3, 5, and 7 days of drug treatment. Six to 9 images were acquired for each specific sample drug treatment, with 1 to 2 images of type 1 organoids (due to their scarcity), 4 to 6 images of type 2 organoids, and 1 to 2 images of fibroblasts. The data from all 3 mouse samples were combined for a total of 5 to 6 images of type 1 organoids (100–600 cells), 12 to 18 images of type 2 organoids (250–800 cells), and 4 to 6 images of fibroblasts (30–100 cells) per drug treatment. Five to 6 human PDAC organoids were imaged per treatment group, for a total number of 100 to 300 cells per treatment.

Immunofluorescence

Immunofluorescence of organoid cultures was performed as previously described.[3,17] First, the growth media were removed from the gels, and the gels were washed with PBS. The PBS was removed, and gels were fixed by submerging in 2 mL of 4% paraformaldehyde in PBS. After 10 minutes, the paraformaldehyde was removed, and gels were washed with PBS. Then, 0.02% Triton X-100 in PBS was added to cover the gels for 10 minutes. Gels were washed with PBS and overlain with 1% fatty acid–free bovine serum albumin and 1% donkey serum in PBS overnight. The next day, the blocking solution was removed from the gels, 100 μL of antibody solution (diluted antibody in PBS with 1% donkey serum) was added to each gel, and gels were incubated at room temperature for 30 minutes. The gels were washed in PBS 3 times and then incubated with the secondary antibody solution for 30 minutes at room temperature. The gels were then washed 3 times with PBS and twice with water. The gels were then mounted on slides using 30 μL of ProLong Antifade Solution (Molecular Probes, Eugene, Oreg).

Cleaved caspase 3 expression was detected with anticleaved caspase 3 primary antibody (Life Technologies, Waltham, Mass). Cell proliferation was detected with anti-Ki67 primary antibody (Life Technologies). Both of these primary antibodies were diluted 1:100. A goat antirabbit IgG Fluorescein isothiocyanate (Life Technologies) secondary antibody was used for imaging contrast. Images of Fluorescein isothiocyanate fluorescence were obtained using the multiphoton microscope with excitation at 980 nm. A minimum of 6 organoids were imaged. Positive staining was confirmed by positive staining of mouse thymus and mouse small intestine for cleaved caspase 3 and Ki67, respectively. Immunofluorescence images were quantified by manual counting the number of positive cells and the total number of cells. Immunofluorescence results are presented as a percentage of positively stained cells, quantified from 6 organoids, approximately 200 cells.

Immunohistochemistry

Gels were scraped and mixed with agarose to create a solid gel for immunohistochemistry processing. The agarose was placed in buffered formalin, paraffin embedded, sliced, and stained with hematoxylin and eosin stains. Additional slides were stained for cytokeratin AE1/AE3.

OMI Data Analysis

Fluorescence lifetime and intensity data were extracted from the fluorescence lifetime images. At each pixel, the fluorescence lifetime decay curve was fit to a 2-component model,

$$I(t) = \alpha_1 \exp\left(-\frac{t}{\tau_1}\right) + \alpha_2 \exp\left(-\frac{t}{\tau_2}\right) + C$$

where $I(t)$ is the fluorescence intensity at time t after the laser excitation pulse, α_1 and α_2 are the fractional contributions of the free and bound molecules (ie, $\alpha_1 + \alpha_2 = 1$), τ_1 and τ_2 are the fluorescence lifetimes of the short and long lifetime components, and C is a constant that accounts for background light. A 2-component model is used because NAD(P)H and FAD can exist in 2 conformation states, bound or unbound, which correspond to short (quenched) and long lifetimes.[5,11,12]

Cytoplasms of cells were segmented from the nuclei and background of autofluorescence organoid images using an automated image segmentation algorithm.[18] Fluorescence lifetime end points, including photon count, α_1, τ_1, and τ_2 are extracted for each cell cytoplasm. Three additional end points, the optical redox ratio (intensity of NAD(P)H–intensity of FAD), the mean NAD(P)H fluorescence lifetime, and the mean FAD fluorescence lifetime were also computed and recorded for each cell cytoplasm. The mean NAD(P)H and mean FAD fluorescence lifetimes were computed from the components, $\tau_m = \alpha_1 \tau_1 + \alpha_2 \tau_2$. A composite end point, the OMI index, was computed from the redox ratio, NAD(P)H τ_m and FAD τ_m. The OMI index is computed for each cell, $\text{OMI Index} = \frac{RRi}{\langle RR \rangle} + \frac{\text{NAD(P)H}\,\tau_{mi}}{\langle \text{NAD(P)H}\,\tau_m \rangle} - \frac{\text{FAD}\,\tau_{mi}}{\langle \text{FAD}\,\tau_m \rangle}$, and is a linear combination of mean-centered redox ratio, NAD(P)H τ_m and FAD τ_m.[3,19] The "OMI index normalized difference" is defined as $\text{OMI}_{ND} = \frac{(\text{OMI}_T - \text{OMI}_C)}{\text{OMI}_C}$, where OMI_{ND} is the OMI index normalized difference, OMI_C is the OMI index of the control-treated organoids, and OMI_T is the OMI index of the drug-treated organoids.

Subpopulation Analysis

Heterogeneity of cellular metabolism was assessed with subpopulation analysis. Each cell population was modeled as a Gaussian mixture distribution model,[3,4,19,20]

$$f(y;\ \Phi_g) = \sum_{i=1}^{g} \pi_i \phi(y;\ \mu_i,\ V_i),$$

where g is the number of components, $\phi\ (y;\ \mu_i,\ V_i)$ represents a normal probability density function with mean μ_i and variance V_i, and π_i is the mixing proportion. ϕ_g represents the unknown parameters (π_i, μ_i, V_i): $i = 1 \ldots g$ in a g-component model. The mixture model was fitted by maximum likelihood using the expectation maximization algorithm to determine the optimum parameters (π, μ, V) (MATLAB, version R2013a; MathWorks, Natick, Mass). Cell populations were modeled 3 times as Gaussian mixture distribution models with 1 to 3 components (g = 1, 2, or 3). The Akaike information criterion is a measure of model goodness of fit and is minimized in the optimal model.[21] The most representative model of the data was selected as the model with the lowest Akaike information criterion. Probability density functions were normalized to have an area under the curve equal to 1.

Statistical Analysis

Time course drug-response OMI data were analyzed with 1-way analysis of variance with a Dunn correction for multiple comparisons between control and drug-treated organoids at each time point. A nonparametric rank sum test with a Bonferroni correction for multiple comparisons was used to assess differences in immunofluorescence results between drug treatments. For all statistical comparisons, an alpha level of 0.05 was used for significance. The number of cells per group varied between 30 and 800. A nonparametric Spearman correlation was performed for correlation analysis between OMI index and immunofluorescence end points for all time points, treatment groups, and cell subtypes pooled together.

RESULTS

Primary ductal adenocarcinoma tumors were mechanically dissociated and grown as organoids in Matrigel. Three distinctive morphologies were observed in murine PDAC organoids (Fig. 1A), including spherical organoids (type 1), asymmetric organoids (type 2), and fibroblasts. Immunohistochemistry analysis revealed that type 1 and 2 organoids were positive for cytokeratin AE1/AE3 (Fig. 1B) and negative for vimentin, CD34, and CD45, indicating an epithelial lineage in agreement with other studies of PDAC organoids.[2] The basal metabolic state varied across the organoid subtypes, with type 1 having the greatest OMI index and type 2 having the smallest OMI index (Fig. 1C). Significant differences in the optical redox ratio indicated a lower redox state in type 2 organoids compared with type 1 and fibroblasts (Fig. 1D). Furthermore, NAD(P)H and FAD fluorescence lifetime analysis revealed significantly shorter NAD(P)H lifetimes in type 2 organoids (Fig. 1E) and longer FAD fluorescence lifetimes (Fig. 1F) compared with type 1 and fibroblasts.

Organoids were treated with G, A1 (JAK2 inhibitor), A6 (MEK inhibitor), X (PI3K inhibitor), and combinations to evaluate drug-induced changes in cellular metabolism. Optical metabolic imaging was performed for 7 days of drug treatment. The time course of drug-induced metabolism changes (Fig. 2A) in type 1 organoids demonstrated an initial reduction in the OMI index on day 1 of A1 treatment ($P < 0.05$) and an increase in the OMI index by days 5 and 7. Gemcitabine induced a metabolic response with a progressive reduction in the OMI index for the entire time course ($P < 0.05$; Fig. 2A). The therapies A6 and XL146, and the combination therapies, A1 + G, A1 + A6 + G, and A1 + A6 + G + X, induced a significant reduction in the OMI index that persisted during the time course ($P < 0.01$; Fig. 2A), with the greatest reductions induced by the combination therapies.

Subpopulation analysis of OMI index data can reveal cell populations with heterogeneous metabolic responses.[19] This analysis revealed that type 1 organoids treated with A1 initially had a bimodal metabolic response to treatment (Fig. 2B). However, this bimodal metabolic response disappeared at later time points, days 3 and 7, revealing the emergence of a distribution that closely matches control.

The time course of drug-induced changes for type 2 organoids showed significant reductions in OMI index due to drug treatment (Fig. 2C). By day 7, the OMI index was significantly reduced because of all single and combination drug treatments ($P < 0.05$; Fig. 2C).

We also assessed drug-induced metabolism changes of the fibroblasts that grew with the organoid cultures. The time course of drug-induced metabolism changes within fibroblasts indicated significant metabolism changes with A1, A6, A1 + G, A1 + A6 + G, and A1 + A6 + G + X treatments (Fig. 2D). Both G and X induced a decrease in the OMI index initially at days 1

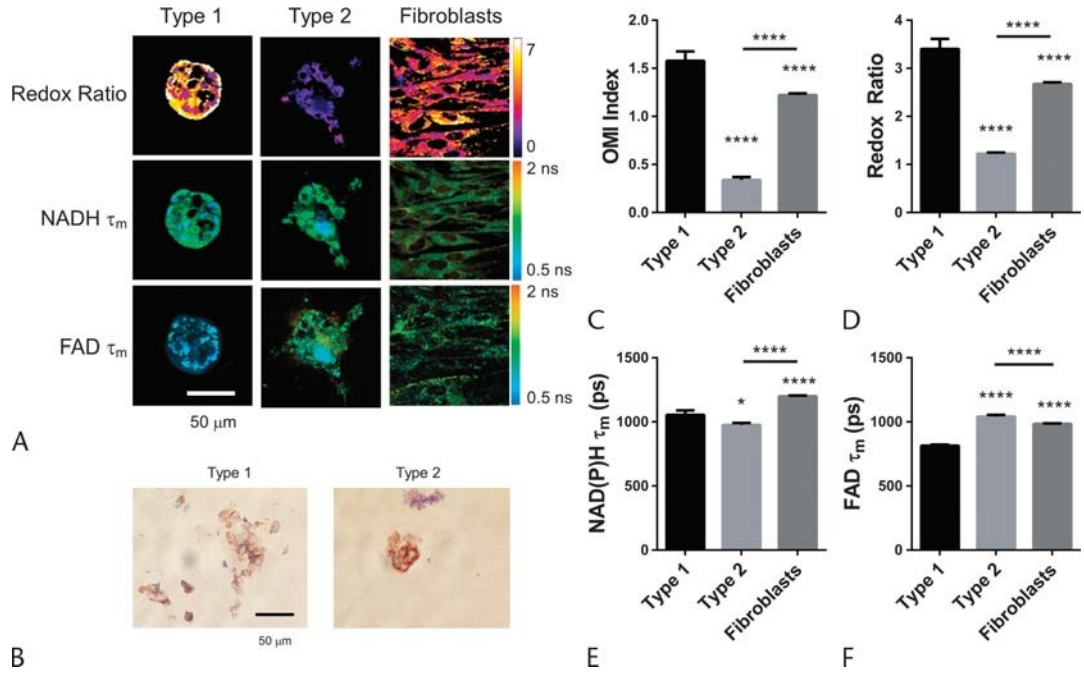

FIGURE 1. A, Representative redox ratio, NAD(P)H τ_m, and FAD τ_m images of murine organoids and fibroblasts. B, Cytokeratin AE1/AE3 staining of murine PDAC types 1 and 2 organoids. C, OMI index. Optical redox ratio (D) (NAD(P)H-FAD), NAD(P)H mean lifetime (E), and FAD mean lifetime (F) of untreated types 1 and 2 organoids and fibroblasts. *$P < 0.05$, ****$P < 0.0001$.

and 2 ($P < 0.05$), but the OMI index reverted to control levels by days 3, 5, and 7 ($P > 0.05$ vs control). Subpopulation analysis of the fibroblasts treated with A1 + A6 + G + X revealed 2 populations of cells on days 1 and 3 of treatment (Fig. 2D) and a single population of cells on day 7. During the time course, the A1 + A6 + G + X population shifts to OMI index values significantly reduced from control cells.

Drug response of the organoids and fibroblasts was confirmed by immunofluorescence staining of cleaved caspase 3 and Ki67 on day 3 (Fig. 3). Correlation analysis revealed the OMI index significantly correlated ($P < 0.05$) with both cleaved caspase 3 and Ki67 staining in the pooled data of both types of organoids and fibroblasts (Fig. 4A), indicating that the OMI index is a robust indicator of drug response. The correlations between

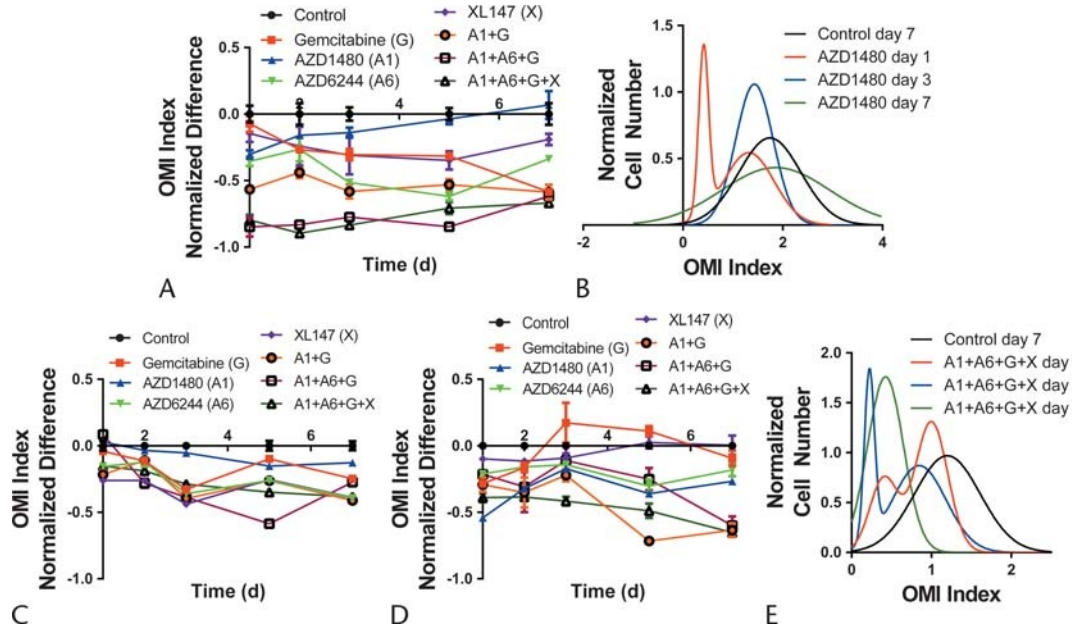

FIGURE 2. A, Time course of drug response for type 1 organoids. B, Subpopulation analysis of A1-treated type 1 organoids. C, Time course of drug response for type 2 organoids. D, Time course of drug response for fibroblasts. E, Subpopulation analysis of fibroblasts treated with A1 + A6 + G + X.

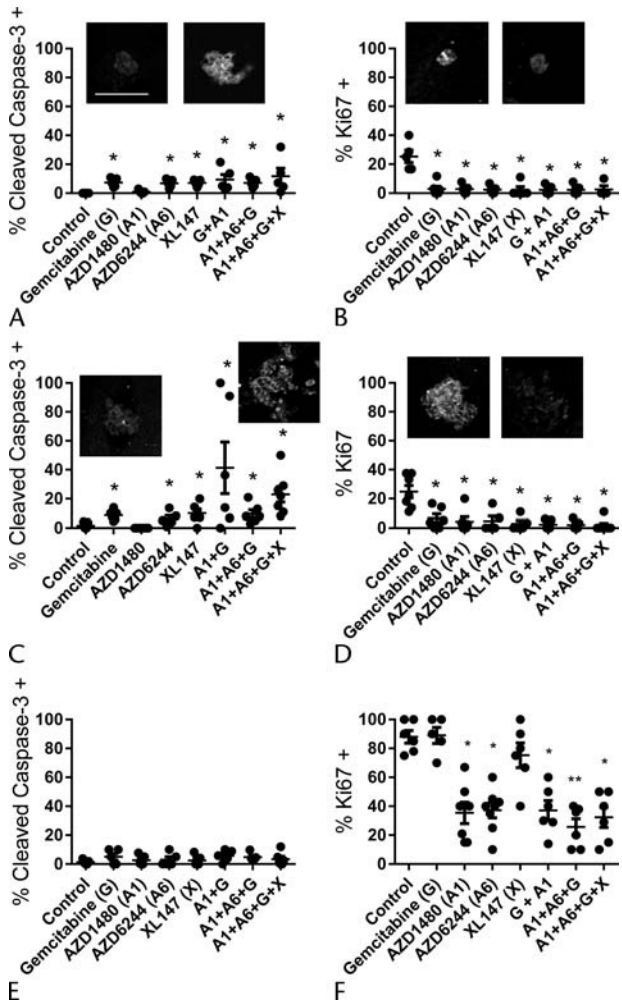

FIGURE 3. Immunofluorescence staining of cleaved caspase 3 and Ki67 for murine PDAC type 1 organoids (A and B), type 2 organoids (C and D), and fibroblasts (E and F), treated with anticancer drugs for 72 hours. Image inserts (A–D) are representative images of control (left) and A1 + G (right) organoids. Scale bar is 50 μm.* $P < 0.05$, **$P < 0.01$.

immunofluorescence and the OMI index within the types 1 and 2 organoids and fibroblasts are also shown (Figs. 4B–D).

To translate this organoid and OMI approach to human tumors, organoids were generated from a primary human PDAC biopsy. Organoids grew robustly from the human PDAC biopsy (Fig. 5A); however, a broad spectrum of organoid morphologies grew that were not easily classified into subtypes. The cells within these organoids stained positive for cytokeratin AE1/AE3, indicating epithelial origin (Fig. 5B). These organoids were treated for 24 hours with G, A1, and A1 + G. A significant reduction in the OMI index was detected with G and A1 + G treatment ($P < 0.01$; Fig. 5C). AZD1480 failed to induce a significant reduction in OMI index in these primary human PDAC organoids at 24 hours.

DISCUSSION

Optical metabolic imaging of PDAC organoids is an attractive platform for studying drug response of novel drugs and for testing specific drugs on patient tissue for individualized treatment decisions. This study investigated the use of an organoid-OMI screen for detecting drug-induced metabolism changes in murine and human PDAC organoids.

We achieved 100% organoid generation rates with mechanical dissociation, with thousands of organoids generated per tissue sample, suggesting robust representation of the majority of cancerous cells in the organoids. Furthermore, the isolation of 2 different morphologies of malignant organoids as well as the growth of fibroblasts indicates isolation and culture of multiple cell types. Although some cell types inherent in the initial tumor tissue may not be represented in the organoids, the organoids morphology matches that of a previous study of PDAC organoid generation.[2] The type 1 organoid morphology matches that of organoids derived from primary PDAC, whereas type 2 matches that of organoids derived from metastatic lesions, suggesting different protein expression and genetics between the 2 organoid types.[2] Our results showed that organoids of differing morphologies could be grown from murine PDAC biopsies (Fig. 1A). Furthermore, in addition to morphological differences, these organoids had varying basal metabolic redox states[7] (Fig. 1D) and differing NAD(P)H and FAD lifetimes indicating differing coenzyme environments and preferred protein binding (Figs. 1E, F).

The drug-response studies indicated that both types 1 and 2 organoids were responsive to the anticancer drugs and combinations (Figs. 2A, C), with the greatest reductions in OMI index due to combination therapies, supporting the use of combination treatments in the clinic. The OMI results suggest similar drug-response behavior between the 2 organoids; however, type 2 shows a response to A1 at days 5 and 7, whereas type 1 develops a resistance to this drug. Furthermore, the subpopulation analysis highlights the use of OMI and demonstrates a dynamic behavior of type 1 organoids, which initially responded to A1 and later regressed by day 7 (Fig. 2B). The immunofluorescence results and correlation analysis (Figs. 3, 4) demonstrate that the OMI index correlates with cell proliferation and death and is an accurate measure of drug response in these PDAC organoids. Notably, no spatial patterns of Ki67 or cleaved caspase 3 staining were observed indicating penetrance of a therapeutic dose of drugs throughout the organoids, in agreement with previous studies of nutrient and drug diffusion in organoids.[22,23] When pooled, the types 1 and 2 and fibroblast immunohistochemistry and OMI index correlated, yet the individual correlations were not all significantly correlated due to the small sample size. Optical metabolic imaging can measure dynamic changes in cellular metabolism within intact, living samples during a time course of drug treatment, which is not possible with destructive immunofluorescence measurements.

Because of the fibrotic nature of PDAC, drug delivery remains a challenge.[24] Although our results demonstrate drug-induced metabolism changes in epithelial tumor cells, these drugs may have limited efficacy in vivo due to hindrance of drug delivery by the extracellular matrix. Several new therapeutic strategies are being investigated to directly target the extracellular matrix and the malignant tumor compartment concurrently.[8,24] Therefore, we also evaluated the metabolism of drug-treated fibroblasts that grew with the PDAC organoids (Fig. 2D). The fibroblasts also showed response to the anticancer drugs with decreased OMI indices and decreased proliferation (Fig. 3F), although the drugs failed to induce significant increases in cell death (Fig. 3E). The lack of fibroblast cell death due to anticancer drugs highlights the challenges of drug delivery to the pancreas, and the organoid-OMI drug screen provides a novel platform to investigate new stromal-targeting drugs.

Organoid drug response matched in vivo drug response of PDAC for a sampling of drugs. Previous studies have found a significant reduction ($P < 0.05$) in tumor volume, and increased

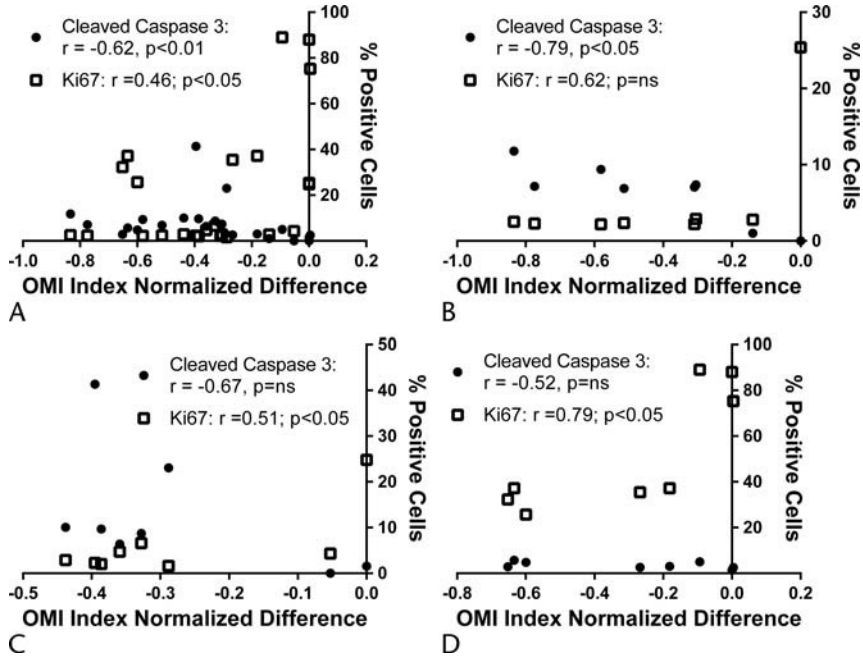

FIGURE 4. A, Correlation analysis of the OMI index versus cleaved caspase 3 and Ki67 staining for both types of organoids and fibroblasts pooled together. Correlation between type 1 (B), type 2 (C), and fibroblast (D) OMI index versus cleaved caspase 3 and Ki67. ns indicates not significant, $P > 0.05$.

survival was observed in PKT mice treated with the combination treatment, A1 + G, compared with control mice or monotherapy mice.[8] For both types 1 and 2 organoids, the OMI index had greater reductions due to combined A1 + G treatment than A1 or G alone (Figs. 2A, C), at all time points, in agreement with in vivo data,[8] indicating that PKT tumors are more responsive to A1 + G treatment than the monotherapies. Furthermore, these previous studies[8] observed enhanced drug delivery in PKT tumors treated with A1 monotherapy and A1 + G. Correlative analysis of the OMI organoid data indicates a significant response of fibroblasts to A1 monotherapy and the combination A1 + G (Fig. 2D), in agreement with the in vivo PKT results,[8] suggesting that OMI measured response of fibroblasts can be used to predict drug delivery of anticancer drugs. Altogether, these results and previously published results in breast cancer[3,4] confirm that OMI measures of organoid drug response provide a robust surrogate measure of in vivo drug response.

Finally, organoids were derived from a human PDAC biopsy (Fig. 5). These results demonstrate that organoids can be grown from primary human PDAC tumors, these organoids exhibit metabolic changes due to anticancer drug treatment, and an organoid-OMI screen can be used to determine drug response with various agents for a short time course (24 hours).

Organoids are an attractive platform for testing drugs on patient-specific tumor tissue for individualized treatment planning and novel drug development. In organoids, malignant epithelial cells can be grown in concert with the tumor-associated fibroblasts and immune cells, which provides a relevant platform to

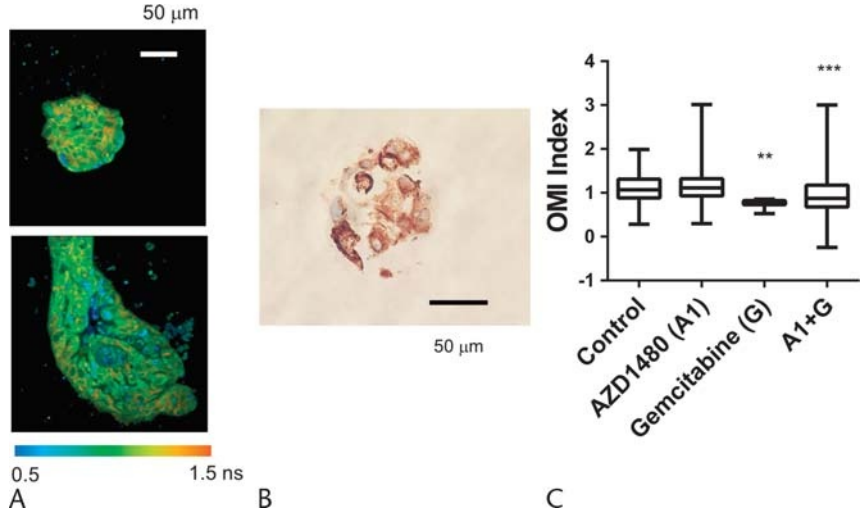

FIGURE 5. A, Representative NAD(P)H τ_m images of human PDAC organoids. B, Cytokeratin AE1/AE3 staining of human PDAC organoid. C, OMI index of human PDAC organoids treated for 1 day. $^{**}P < 0.01$, $^{***}P < 0.001$.

study cell-cell interactions and drug effects based on the entire tumor microenvironment. This is particularly important for PDAC as drug efficacy can be impaired by the tumor stroma. Here, we present novel findings of differential drug responses in different subpopulations of tumor cells and in tumor-associated fibroblasts within the same cultures. In addition, we demonstrate a novel imaging technique, OMI, which is highly sensitive to detecting early drug-induced changes in cellular metabolism within intact, living samples. We have also shown that these changes in cellular metabolism correlate with changes in cell proliferation and cell death, indicating that cellular metabolism can be a surrogate measure of drug response. These findings have significant implications for rapidly assessing therapeutic response in patient pancreatic tumors.

REFERENCES

1. Cheung KJ, Gabrielson E, Werb Z, et al. Collective invasion in breast cancer requires a conserved basal epithelial program. *Cell*. 2013;155:1639–1651.
2. Boj SF, Hwang CI, Baker LA, et al. Organoid models of human and mouse ductal pancreatic cancer. *Cell*. 2015;160:324–338.
3. Walsh AJ, Cook RS, Sanders ME, et al. Quantitative optical imaging of primary tumor organoid metabolism predicts drug response in breast cancer. *Cancer Res*. 2014;74:5184–5194.
4. Walsh AJ, Cook RS, Manning HC, et al. Optical metabolic imaging identifies glycolytic levels, subtypes, and early-treatment response in breast cancer. *Cancer Res*. 2013;73:6164–6174.
5. Skala MC, Riching KM, Gendron-Fitzpatrick A, et al. In vivo multiphoton microscopy of NADH and FAD redox states, fluorescence lifetimes, and cellular morphology in precancerous epithelia. *Proc Natl Acad Sci U S A*. 2007;104:19494–19499.
6. Chance B, Schoener B, Oshino R, et al. Oxidation-reduction ratio studies of mitochondria in freeze-trapped samples. NADH and flavoprotein fluorescence signals. *J Biol Chem*. 1979;254:4764–4771.
7. Varone A, Xylas J, Quinn KP, et al. Endogenous two-photon fluorescence imaging elucidates metabolic changes related to enhanced glycolysis and glutamine consumption in precancerous epithelial tissues. *Cancer Res*. 2014;74:3067–3075.
8. Nagathihalli NS, Castellanos JA, Shi C, et al. Signal Transducer and Activator of Transcription 3, Mediated Remodeling of the Tumor Microenvironment Results in Enhanced Tumor Drug Delivery in a Mouse Model of Pancreatic Cancer. *Gastroenterology*. 2015;149:1932–1943.e9.
9. Walsh AJ, Poole KM, Duvall CL, et al. Ex vivo optical metabolic measurements from cultured tissue reflect in vivo tissue status. *J Biomed Opt*. 2012;17:116015.
10. Georgakoudi I, Quinn KP. Optical imaging using endogenous contrast to assess metabolic state. *Annu Rev Biomed Eng*. 2012;14:351–367.
11. Lakowicz J. *Principles of Fluorescence Spectroscopy*. New York, NY: Plenum Publishers; 1999.
12. Lakowicz JR, Szmacinski H, Nowaczyk K, et al. Fluorescence lifetime imaging of free and protein-bound NADH. *Proc Natl Acad Sci U S A*. 1992;89:1271–1275.
13. Tanaka F, Tamai N, Yamazaki I. Picosecond-resolved fluorescence spectra of D-amino-acid oxidase. A new fluorescent species of the coenzyme. *Biochemistry*. 1989;28:4259–4262.
14. Walsh A, Cook RS, Rexer B, et al. Optical imaging of metabolism in HER2 overexpressing breast cancer cells. *Biomed Opt Express*. 2012;3:75–85.
15. Skala MC, Riching KM, Bird DK, et al. In vivo multiphoton fluorescence lifetime imaging of protein-bound and free nicotinamide adenine dinucleotide in normal and precancerous epithelia. *J Biomed Opt*. 2007;12:024014.
16. Huang S, Heikal AA, Webb WW. Two-photon fluorescence spectroscopy and microscopy of NAD(P)H and flavoprotein. *Biophys J*. 2002;82:2811–2825.
17. Wozniak MA, Keely PJ. Use of three-dimensional collagen gels to study mechanotransduction in T47D breast epithelial cells. *Biol Proced Online*. 2005;7:144–161.
18. Walsh AJ, Skala MC. An automated image processing routine for segmentation of cell cytoplasms in high-resolution autofluorescence images. *SPIE Proceedings*. 2014;8948.
19. Walsh AJ, Skala MC. Optical metabolic imaging quantifies heterogeneous cell populations. *Biomed Opt Express*. 2015;6:559–573.
20. Pan W, Lin J, Le CT. Model-based cluster analysis of microarray gene-expression data. *Genome Biol*. 2002;3:RESEARCH0009.
21. Akaike H. A new look at the statistical model identification. *IEEE Trans Automat Control*. 1974;19:716–723.
22. Achilli TM, McCalla S, Meyer J, et al. Multilayer spheroids to quantify drug uptake and diffusion in 3D. *Mol Pharm*. 2014;11:2071–2081.
23. Mueller-Klieser W. Method for the determination of oxygen consumption rates and diffusion coefficients in multicellular spheroids. *Biophys J*. 1984;46:343–348.
24. Provenzano PP, Cuevas C, Chang AE, et al. Enzymatic targeting of the stroma ablates physical barriers to treatment of pancreatic ductal adenocarcinoma. *Cancer Cell*. 2012;21:418–429.